Structural characterization of an ATPase active F-1-/V-1-ATPase (alpha(3)beta(3)EG) hybrid complex

Chaban, Yuriy L.; Coskun, Ünal; Keegstra, Wilko; Oostergetel, Gert T.; Boekema, Egbert J.; Grüber, Gerhard

Published in:
The Journal of Biological Chemistry

DOI:
10.1074/jbc.m408460200

Publication date:
2004

THE JOURNAL OF BIOLOGICAL CHEMISTRY
Vol. 279, No. 46, Issue of November 12, pp. 47866–47870, 2004
Printed in U.S.A.

Structural Characterization of an ATPase Active F_1-/V_1-ATPase ($\alpha_3\beta_3$EG) Hybrid Complex*

Received for publication, July 26, 2004, and in revised form, September 2, 2004
Published, JBC Papers in Press, September 8, 2004, DOI10.1074/jbc.M408460200

Yuriy L. Chaban‡, Ünal Coskun§, Wilko Keegstra‡, Gert T. Oostergetel‡, Egbert J. Boekema‡¶, and Gerhard Grüber§‖

From the ‡Department of Biophysical Chemistry, Groningen Biomolecular Sciences and Biotechnology Institute, University of Groningen Nijenborgh 4, 9747 AG Groningen, The Netherlands and §Universität des Saarlandes, Fachrichtung 2.5-Biophysik, D-66421 Homburg, Germany

Co-reconstitution of subunits E and G of the yeast V-ATPase and the α and β subunits of the F_1-ATPase from the thermophilic *Bacillus* PS3 (TF_1) resulted in an $\alpha_3\beta_3$EG hybrid complex showing 53% of the ATPase activity of TF_1. The $\alpha_3\beta_3$EG oligomer was characterized by electron microscopy. By processing 40,000 single particle projections, averaged two-dimensional projections at 1.2–2.4-nm resolution were obtained showing the hybrid complex in various positions. Difference mapping of top and side views of this complex with projections of the atomic model of the $\alpha_3\beta_3$ subcomplex from TF_1 (Shirakihara, Y., Leslie, A. G., Abrahams, J. P., Walker, J. E., Ueda, T., Sekimoto, Y., Kambara, M., Saika, K., Kagawa, Y., and Yoshida, M. (1997) *Structure* 5, 825–836) demonstrates that a seventh mass is located inside the shaft of the $\alpha_3\beta_3$ barrel and extends out from the hexamer. Furthermore, difference mapping of the $\alpha_3\beta_3$EG oligomer with projections of the A_3B_3E and A_3B_3EC subcomplexes of the V_1 from *Caloramator fervidus* (Chaban, Y., Ubbink-Kok, T., Keegstra, W., Lolkema, J. S., and Boekema, E. J. (2002) *EMBO Rep.* 3, 982–987) shows that the mass inside the shaft is made up of subunit E, whereby subunit G was assigned to belong at least in part to the density of the protruding stalk. The formation of an active $\alpha_3\beta_3$EG hybrid complex indicates that the coupling subunit γ inside the $\alpha_3\beta_3$ oligomer of F_1 can be effectively replaced by subunit E of the V-ATPase. Our results have also demonstrated that the E and γ subunits are structurally similar, despite the fact that their genes do not show significant homology.

Vacuolar-type ATPases (V-ATPases)[1] are membrane-bound proteins functioning in active ion pumping at the expense of ATP hydrolysis. They are present in the membranes of all eukaryotic cells and the plasma membrane of some bacteria (1–3). V-ATPases are responsible for acidification of intracellular compartments and generation of an electrochemical gradient (ion motive force) (4, 5). These enzymes consist of two structural and functional parts, a hydrophilic, V_1, and hydrophobic, V_O, portion. The V_1 part contains eight (A-H) and seven subunits (A-G) in the cases of the eukaryotic and prokaryotic enzymes, respectively (3, 4). V_O in eukaryotes consists of subunits a, c, and d, corresponding to subunits I, K, and C in prokaryotic V-ATPases (*Enterococcus hirae* nomenclature). Phylogenetic (6, 7), biochemical (8), and structural studies of V-ATPases (reviewed in Refs. 3, 9, and 10) show its relation to the well characterized F-ATPases (11, 12). Because of the structural similarity, it is believed that the energy-coupling mechanism of ATP hydrolysis and ion translocation is similar to that in F-ATPases (13). Therefore, the ATP hydrolysis in the A_3B_3 hexamer of V_1 might trigger the rotational movement(s) of the central stalk subunit(s). Rotation of the central stalk transfers a generated torque to the ring of the c (K) subunits in the V_O part (13), resulting in the pumping of ions over the membrane. The stability of the A_3B_3 hexamer against rotation is provided by peripheral stalk(s) connecting static subunits of V_1 and V_O.

Despite assigned similarity in the catalytic mechanism, a growing amount of evidence suggests that some structural features and regulatory mechanisms of both enzymes are different, reflecting diversities in their functions and evolution (for review, see Ref. 14). The most significant structural difference is shown in the stalk(s) region. Unlike F-ATPases, where the presence of only one peripheral stalk was reported (15, 16), two or three peripheral stalks were described for the V-ATPase (17–19). The structure of the central stalk in the V-ATPase also seems to be more complicated. Electron microscopy (20) and small angle x-ray scattering studies (21) indicated that the central stalk of V-ATPase is rather elongated when compared with that in the F-ATPase. The exact assignment of the subunits involved in these stalk region formations is a matter of debate, and it is difficult to identify the V-ATPase stalk subunits that have significant sequence similarity to the stalk subunits of the F-ATPase (3). According to secondary structure prediction, the V-ATPase subunits D and E can be candidates for the homologue role of the rotating γ subunit in F-ATPase (22, 23). Experiments on assembly of the V-ATPase from yeast indicate that either the D or E subunits, or both, might be a functional homologue of subunit γ (24). Recently, hydrolytically active A_3B_3EC and A_3B_3EG subcomplexes from *Caloramator fervidus* (25) and *Manduca sexta* (26) V-ATPase, respectively, were visualized by electron microscopy showing that subunit E is part of the central stalk. In addition, a hydrolytically active $\alpha_3\beta_3$E hybrid complex, composed of the α and β subunits of the thermophilic F-ATPase and subunit E (Vma4p) of the *Saccha-*

* This work was supported by Deutsche Forschungsgemeinschaft Grants GR 1475/9–1 and GR 1475/9–2 (to G. G.) and by the Dutch Scientific Foundation NWO/CW (to E. J. B.). The costs of publication of this article were defrayed in part by the payment of page charges. This article must therefore be hereby marked "*advertisement*" in accordance with 18 U.S.C. Section 1734 solely to indicate this fact.

¶ To whom correspondence may be addressed: Dept. of Biophysical Chemistry, Groningen Biomolecular Sciences and Biotechnology Institute, University of Groningen Nijenborgh 4, 9747 AG Groningen, The Netherlands. Tel.: 31/(0)50-363-4225; Fax: 31/(0)50-363 4800; E-mail: boekema@chem.rug.nl.

‖ To whom correspondence may be addressed: Universität des Saarlandes, FR 2.5-Biophysik, Universitätsbau 76, D-66421 Homburg, Germany. Tel.: 49/(0)6841-162-6085; Fax: 49/(0)6841-162-6086; E-mail: ggrueber@uniklinik-saarland.de.

[1] The abbreviations used are: V-ATPase, vacuolar-type ATPase; F-ATPase, F_1Fo-ATP synthase; TF_1, F_1-ATPase from *Bacillus* strain PS3; MRA, multireference alignment.

romyces cerevisiae V-ATPase, could be assembled, indicating a major role of subunit E in ATP hydrolysis (27).

We have now turned our attention to the first structural determination of a larger ATPase active F_1/V_1 hybrid complex, $\alpha_3\beta_3$EG. This complex also contains the V-ATPase subunit G (Vma10p), which has been proposed to be essential for the assembly and activity of the V-ATPase (24, 28, 29). The position of the E and G subunits in this hybrid complex was determined after single particle image analysis compared with projections of the $\alpha_3\beta_3$ molecular model of TF_1- (30) and V_1-ATPase subcomplexes from *C. fervidus* (25).

EXPERIMENTAL PROCEDURES

Materials—Nickel-nitrilotriacetic acid chromatography resin was received from Qiagen (Hilden, Germany). Chemicals for gel electrophoresis were purchased from Serva (Heidelberg, Germany). All other chemicals were at least of analytical grade and received from BIOMOL (Hamburg, Germany), Merck, Roth (Karlsruhe, Germany), Sigma, or Serva (Heidelberg, Germany).

Protein Preparation—The α and β subunits of F_1-ATPase from the thermophilic *Bacillus* strain PS3 were purified as described previously (31) and were a generous gift from Prof. M. Yoshida (Tokyo Institute of Technology, Yokohama, Japan). Both subunits were precipitated by adding solid ammonium sulfate and were then dissolved in buffer A containing 50 mM Tris/HCl (pH 8.0) and 100 mM NaCl. The final protein concentration of each subunit was 50 mg/ml. The complete TF_1, isolated according to Kagawa and Yoshida (32), was a generous gift from Prof. H.-J. Schäfer (Johannes-Gutenberg Universität, Mainz, Germany). Subunits E (Vma4p) and G (Vma10p) of the *S. cerevisiae* V-ATPase were expressed and purified according to Grüber *et al.* (27) and Armbrüster *et al.* (33), respectively. To form an $\alpha_3\beta_3$G or an $\alpha_3\beta_3$EG hybrid complex, subunit G or subunits E and G were mixed with subunit α and β subunits of TF_1 and dialyzed overnight at 4 °C against buffer A using a 300-kDa Spectra/Por dialysis membrane (Spectrum Laboratories). The incubated mixture was applied on a Sephacryl™ S-300 HR 10/30 column (Amersham Biosciences) and eluted with 50 mM Tris/HCl (pH 8.0) and 150 mM NaCl. The peak fractions were collected and analyzed by SDS-PAGE (34) and native gel electrophoresis (35) and stained with Coomassie Brilliant Blue G250. Mg^{2+}-dependent ATPase activity was determined by continuous measurements of the liberated phosphate at 60 °C as described earlier (36).

Electron Microscopy and Image Analysis—Samples of purified complexes were negatively stained using the droplet method with 2% uranyl acetate on glow discharged carbon-coated copper grids. Electron microscopy was performed on a Philips CM 20 FEG electron microscope operated at 200 kV. Images of 4,096 × 4,096 pixels were recorded at ×67,200 magnification at a pixel size of 15 mm with a Gatan 4000 SP 4K slow-scan CCD camera, with "GRACE" software for semi-automated specimen selection and data acquisition (37). Single particle analysis was performed with the Groningen image processing ("GRIP") software package on a PC cluster.[2] A total of 40,000 single particle projections (160 × 160 pixel frame; pixel size 0.23 nm) from 147 images was obtained by selecting all discernable particles. For each micrograph the defocus value was determined, and a simple contrast transfer function correction by phase reversal was done (38). For the alignment of the projections, multireference alignment (MRA) and a reference-free alignment by classification (39) were used. Particles were then subjected to multivariate statistical analysis (MSA) (40) followed by hierarchical ascendant classification (HAC) (41). The cycle consisting of MRA, MSA, and HAC was repeated until stable classes were formed. Alternatively, 42 projections of the atomic model of the $a_3\beta_3$-TF_1 (Protein Data Bank accession code 1SKY) (30) were used as references for MRA. The set of the atomic model projections at a truncated resolution of 1.8 nm was generated using routines from the EMAN software package (42). The aligned class averages were compared with the corresponding projections of the TF_1 $a_3\beta_3$ atomic model and side view projections of the V_1-ATPase subcomplexes from the thermophilic bacterium *C. fervidus* (25). Selection of the atomic model projections was done on the basis of correlation coefficients obtained after alignment of 187 projections to the electron microscopy projection, the shape of the complexes, and relative position of the electron density peaks. The resolution of the class averages was measured according to Ref. 43.

[2] W. Keegstra, unpublished information.

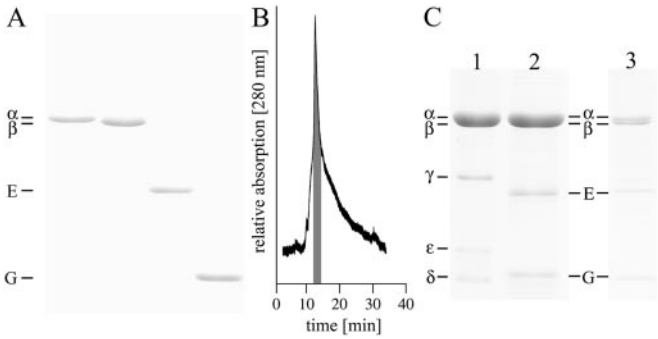

FIG. 1. **Purification and subunit analysis of the $\alpha_3\beta_3$EG hybrid complex.** *A*, SDS-PAGE of the isolated subunits α, β, E (Vma4p), and G (Vma10p). *B*, subunits α, β, E (Vma4p), and G (Vma10p) were incubated as described under "Experimental Procedures" and applied onto a Sephacryl™ S-300 HR column eluted with 50 mM Tris/HCL (pH 8.0) and 150 mM NaCl. *C*, the indicated fractions from panel *B* (▨) were pooled and subjected (*lane 2*) to a gradient SDS-PAGE (12–16%) and stained with Coomassie Blue G250. *Lane 1*, 2 μg of TF_1. *Lane 3*, to show the different apparent molecular masses of the α and β subunits, the pooled fraction of *lane 2* was diluted with 50 mM Tris/HCL (pH 8.0) and 150 mM NaCl.

RESULTS

Reconstitution of an $a_3\beta_3$EG or $a_3\beta_3$G Hybrid Complex—Recent work has shown that an $\alpha_3\beta_3$E hybrid complex, consisting of the major α and β subunits of the thermophilic F_1-ATPase (TF_1) and V-ATPase subunit E (Vma4p) from *S. cerevisiae*, can be assembled that is functional in ATP hydrolysis (27). To test whether an enlarged active $\alpha_3\beta_3$EG hybrid complex can be formed, the isolated α and β subunits of TF_1 together with subunits E (Vma4p) and G (Vma10p) (Fig. 1*A*) were incubated overnight at high concentrations. Subsequent size exclusion chromatography resulted in an elution profile with a main peak at 13 min (Fig. 1*B*). The fractions of this major peak were pooled and analyzed by SDS-PAGE (Fig. 1*C*). The obtained complex comprises the subunits α, β, E, and G. To demonstrate that the pooled fractions (Fig. 1, ▨) contain the $\alpha_3\beta_3$EG complex and no further $\alpha_3\beta_3$E, $\alpha_3\beta_3$G, or $\alpha_3\beta_3$ complexes, the collected fractions were applied onto a Native-PAGE (Fig. 2*A*, *lane 2*). The $\alpha_3\beta_3$EG complex runs as a single band on the native gel. By comparison, the $\alpha_3\beta_3$ complex runs significantly faster in the Native-PAGE (Fig. 2*A*, *lane 1*), indicating that the polled fractions include only highly mono disperse $\alpha_3\beta_3$EG complexes (*lane 2*). The single band of lane 2, analyzed by a second dimension SDS-PAGE (Fig. 2*B*, *lane 2*), contains all four subunits of the $\alpha_3\beta_3$EG hybrid complex identified above. The ATPase activity of the $\alpha_3\beta_3$EG complex is 29 ± 2 μmol ATP hydrolyzed/min/mg. By comparison, for the $\alpha_3\beta_3$ and $\alpha_3\beta_3$E complexes and the complete TF_1-ATPase, a specific activity of 11 ± 3 μmol ATP hydrolyzed/min/mg, 31 ± 2 μmol ATP hydrolyzed/min/mg (27), and 54 ± 3 μmol ATP hydrolyzed/min/mg, respectively, was measured.

In contrast, the incubation of the subunits α and β and subunit G (Vma4p) under the same conditions as described for the reconstitution of an $\alpha_3\beta_3$E (27) or an $\alpha_3\beta_3$EG hybrid complex (see above) resulted in the formation of an $\alpha_3\beta_3$ complex without subunit G (data not shown).

Electron Microscopy and Image Analysis—To investigate the structure of the $\alpha_3\beta_3$EG hybrid complex, a data set of 40,000 electron microscopy single particle projections was used. The data set was first analyzed as 160 × 160 pixel frames in four parts. The initial classifications revealed that about 60% of the single particle projections represented well recognizable top view features, and the remaining 40% represented other views. It allowed us to separate all projections into two new subsets, which were further processed separately. Because of the

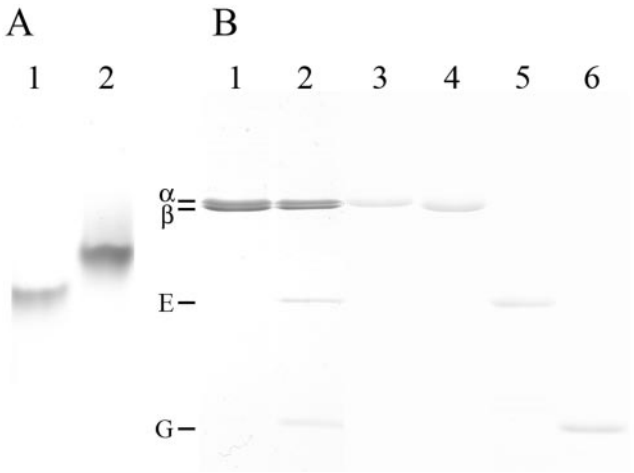

FIG. 2. **Native-PAGE and SDS-PAGE of the $\alpha_3\beta_3$EG hybrid complex.** *A*, the indicated fractions (▨) of the elution profile in Fig. 1*B* were applied to a native polyacrylamide gel (4–15%; Bio-Rad) (*lane 2*). *Lane 1*, an $\alpha_3\beta_3$ complex. The single bands in *lanes 1* and *2* were cut out, destained, and divided into small pieces. After addition of dissociation buffer with 20 mM dithiothreitol, gel pieces were heated at 95 °C for 10 min and centrifuged for 5 min at 13,500 rpm. *B*, the supernatant was applied instantly to an SDS-polyacrylamide gel (12–16%). *Lanes 1* and *2* correspond to the supernatant of bands 1 and 2 of the Native-Page (Fig. 1*A*), respectively. Subunits α, β, E (Vma4p), and G (Vma10p) was applied in *lanes 3-6*, respectively.

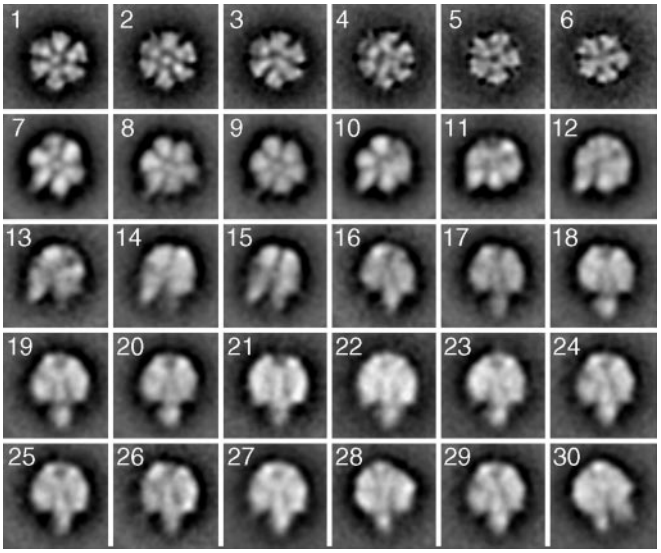

FIG. 3. **A gallery of selected classes from the analysis of 40,000 projections of the $\alpha_3\beta_3$EG hybrid complex.** *Classes 1–9* represent top view projections, *16–30* represent side views, and *10–15* are considered intermediate projections.

smaller size of the top view projections, analysis of the 18,000 projections together could be performed after a reduction of the box size. After several subsequent cycles of MRA, multivariate statistical analysis, and hierarchical ascendant classification, a resolution of 1.2–1.4 nm was achieved for the top view class averages. Images 1–6 (Fig. 3) represent some typical class averages from this data set. The well resolved top view averages 1 and 2, as well as the similar lower resolution images 7–9 (see below), show projections with six major densities in a pseudo 6-fold arrangement plus a seventh central density. This seventh density is not clearly seen in the case of images 3, 4, and 10, probably because of overlap with peripheral densities. Surprisingly, a number of top view projections with a smaller diameter were found in images 5 and 6. In these averages only five instead of six large peripheral densities were present and without a distinct central density.

The box size of images comprising the second data set of the remaining 40% of projections could not be significantly reduced. Instead, a 2 × 2 binning was applied on the images, resulting in a new pixel size of 0.46 nm. This allowed an MRA on more than 20,000 projections simultaneously. A set of 42 projections of the atomic model of the $a_3\beta_3$ subcomplex of TF_1 was used as reference set for an MRA on these data (see "Experimental Procedures"). As a result, stable class averages were obtained with a resolution between 1.8 and 2.4 nm (Fig. 3, *7–30*). Among the 20,000 projections, some turned out to be clustered in classes with top views (*images 7–9*). Other projections represent intermediate positions of the complex between top and side views (*images 10–15*) or side views of the complex (*images 16–30*).

To determine the precise location of the additional mass in the $\alpha_3\beta_3$EG hybrid a comparison with $\alpha_3\beta_3$ particles would be obvious, but unfortunately such particles do not yield significant numbers of side view projections in electron microscopy specimens. Therefore, the best corresponding projections of the $\alpha_3\beta_3$-TF_1 atomic model (Fig. 4, *A–O*) were used for difference mapping with the $\alpha_3\beta_3$EG hybrid complex. Difference mapping between top views shows the presence of additional mass in the central part of the complex (Fig. 4, *A–F*). In the case of one of the intermediate projections, the density is seen in the lower left part of the complex (Fig. 4, *G–I*). Comparison of the side views shows a prominent additional density below the $\alpha\beta$ trimer that continues in the direction of the catalytic shaft (Fig. 4, *J–L*). This density is also prominent in the difference map of Fig. 4*O*. The map, however, also suggests that some molecules appear larger in size in side view position, as can be seen from density at the periphery of the $\alpha_3\beta_3$ head part.

Attempts were made to correlate the side view projections of the $\alpha_3\beta_3$EG hybrid complex to side view projections of the negatively stained V_1 subcomplexes A_3B_3E and A_3B_3EC from the bacterium *C. fervidus* (25). When the side view of the A_3B_3E subcomplex of the *C. fervidus* V-ATPase (Fig. 4*Q*) is subtracted from the one of the $\alpha_3\beta_3$EG hybrid complex views (*P*), a prominent density in the lower left part of the central stalk region remains (*R*). Finally, when the $\alpha_3\beta_3$EG hybrid complex (Fig. 4*T*) is subtracted from the A_3B_3EC subcomplex of the *C. fervidus* V-ATPase (*S*), a prominent density at the tip of the central stalk region remains (*U*). However, comparison shows that the density of *panel R* does not coincide with that of *panel U*, which was determined to be subunit C of *C. fervidus* (25). The difference map of *panel U* identifies also two additional features on top of the V-ATPase subcomplex A_3B_3EC.

DISCUSSION

Single particle analysis resulted in the visualization of projections of the $\alpha_3\beta_3$EG hybrid complex in different orientations. The density maps of this complex (Fig. 3, *1–9*) show a central density surrounded by six peripheral densities, which resembles those of the central stalk subunits of F- and V-ATPases (25, 44). Similar to the top views, the appearance of the side view averages strongly suggests the presence of the central stalk subunit(s) in the $\alpha_3\beta_3$EG complex. The assumption that the central stalk density belongs to the V-ATPase subunits E and G is demonstrated by the difference mapping between the hybrid complex and $\alpha_3\beta_3$ TF_1 projections (Fig. 4, *A–O*). The presence of the additional density in the catalytic shaft of the $\alpha_3\beta_3$ hexamer is clearly depicted in Fig. 4, *C*, *F*, *L*, and *O*.

In this context, the finding of top view projections with five large densities is of interest. The similarity to the particles with six large densities allows us to suggest that the particles represent complexes with misassembled α and/or β subunits. It seems that these complexes lack the central density so promi-

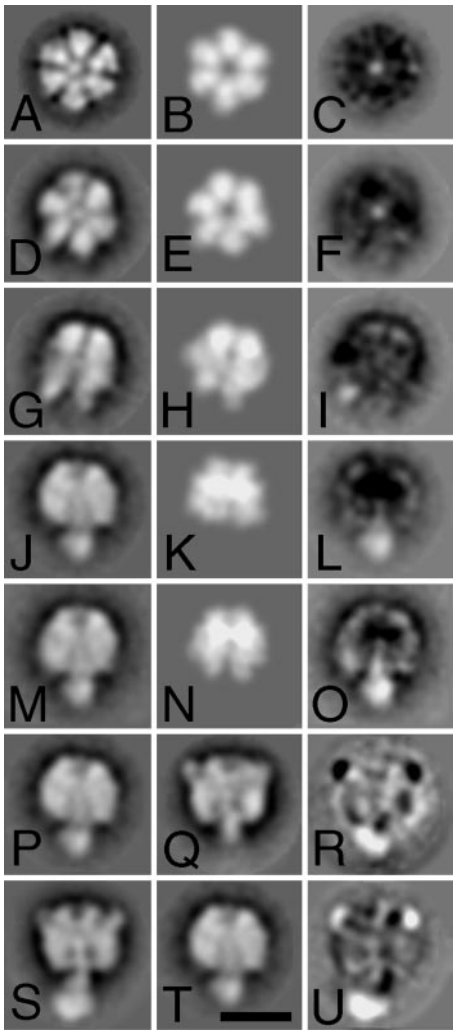

FIG. 4. **Comparison of the $\alpha_3\beta_3$EG hybrid complex with projections of $\alpha_3\beta_3$ hexamer from TF_1 (30) and of the A_3B_3E and A_3B_3EC complexes from the *C. fervidus* V-ATPase (25).** Selected views (*D*, *G*, *J*, *M*, *P*, *S*) of the hybrid ATPase from Fig. 3 were compared with projections (*B*, *E*, *H*, *K*, *N*) of the atomic model of TF_1 (30). Difference maps of the horizontal pairs indicate additional mass present in the hybrid (*bright areas*, *C*, *F*, *I*, *L*, *O*). A further comparison with the A_3B_3E (*panel Q*) and A_3B_3EC complexes (*panel S*) from the *C. fervidus* V-ATPase indicates that the central stalk of the hybrid has an additional mass between the previously reported E and C subunits (25) (r = P−Q, U = S−T). The *bar* corresponds to 10 nm.

nent in the case of the particles with six densities. The number of the projections with pseudo 5-fold symmetry was estimated as 10% within the group of top views. However, we have seen for various V_1-ATPase fragments that the ratio between top and side view projections is proportional to the length of the stalk and can be very high in the case of the particles without stalks (25). This explains the absence of distinct side views of molecules with five large subunits and indicates that the actual number of such molecules would probably be very low.

Nevertheless, from the difference maps of the $\alpha_3\beta_3$EG hybrid and $\alpha_3\beta_3$ subcomplex some fuzzy mass surrounding the $\alpha_3\beta_3$ hexamer of $\alpha_3\beta_3$EG hybrid can be seen (Fig. 4). The slightly larger size of the $\alpha_3\beta_3$EG hybrid complex in the electron microscopy projection, compared with the feature of the $\alpha_3\beta_3$ crystal structure, is probably because of flattening effects during the sample preparation, as recently described for the superposition of the bovine F_1 profiles from electron micrographs and the outline of the crystal structure of the same enzyme (45). Besides this interpretation, it is possible that such alterations might be caused by the introduction of the central stalk subunits in the catalytic shaft of the $\alpha_3\beta_3$ hexamer. As demonstrated by the atomic model of the $\alpha_3\beta_3$ oligomer of TF_1, the hexamer has an exact 3-fold symmetry in the absence of the central subunit γ (30), whereby the symmetry in F-and V-ATPases can be altered by the presence of the central stalk subunit(s) (47, 48). Such structural alterations due to the absence or presence of the central stalk region are in line with the functional changes of these complexes. The $\alpha_3\beta_3$ hexamer hydrolyzes ATP at rates approaching 20% (this study) to 25% (49) of the V_{max} of the complete TF_1. By comparison, the $\alpha_3\beta_3$EG hybrid complex has 54% of the ATPase activity of the native TF_1. In addition, as previously demonstrated, the F_1/V_1 hybrid complex, consisting of the $\alpha_3\beta_3$E-oligomer, showed 57% of total TF_1-ATPase activity (27). Taken together, the results imply that subunit E is essential for ATPase function of the complex.

While the difference mapping with the TF_1 subcomplex indicates the presence of the additional mass in the central stalk region, which can be assigned to the V-ATPase E and G subunits, comparison with the A_3B_3E and A_3B_3EC subcomplexes of V_1 from *C. fervidus* (25) enables determination of the position of these subunits within the V_1 complex. Fig. 4*R* reveals that the upper part of the $\alpha_3\beta_3$EG complex corresponds well to the A_3B_3E fragment from *C. fervidus*. At the same time, a relatively large additional density is present in the lower part of the $\alpha_3\beta_3$EG complex. The size and position of this density differs from the previously described stalk region of subunit C in the A_3B_3EC oligomer from the *C. fervidus* V-ATPase (25) as it is depicted in Fig. 4*U*. Therefore, this density can indicate the presence of subunit G. Such close proximity of subunit G to E has been described from binding (24) and zero-length cross-link experiments (50). In line with these findings are the most recent data of the V_1-ATPase from *M. sexta* demonstrating that the "core" complex consists at least of the four subunits A, B, E, and G and that it still retains 58% of hydrolytic ATPase activity (26). Averaged projections of this core complex show a hexagonal arrangement of the major subunits A and B surrounding a seventh mass composed of both subunits E and G. Furthermore, subunit G of the yeast vacuolar ATPase exists in solution as an elongated dimer (8.0 ± 0.3 nm) (33). It has been proposed from recent studies using a bifunctional cross-link reagent that subunit G is located at the outer surface of subunit B of the yeast V-ATPase (51). From the data in this study it is not obvious if subunit G forms a dimer in the hybrid complex and whether G might span the length of the stalk and extend to the nucleotide binding subunit B. In this context it should be realized that other small subunits that could be important for the position of the G subunit(s) are absent. Nevertheless, the difference maps presented demonstrate that subunit G belongs at least in part to the tip of the central stalk of the $\alpha_3\beta_3$EG hybrid complex. Such an arrangement of subunit G in the central stalk is not surprising, because cross-linking experiments in the V_1-ATPase from yeast (24), clathrin-coated vesicles (51), and *M. sexta* (50) demonstrated that subunit G is in close proximity to subunit F, which is proposed to form a part of the bottom in the central stalk of the complete V_1 (4). Finally, the fact that $\alpha_3\beta_3$, $\alpha_3\beta_3$E, and $\alpha_3\beta_3$EG hybrid complexes, but not $\alpha_3\beta_3$G complex, can be formed by the use of the same reconstitution protocol further supports the view that subunit G is bound to the $\alpha_3\beta_3$EG complex via subunit E.

The difference map of the A_3B_3EC complex from *C. fervidus* with the $\alpha_3\beta_3$EG hybrid complex indicates two extended densities protruding from the V_1 oligomer (Fig. 4*U*). Protrusions on the upper part of the V_1 headpiece are also shown in the three-dimensional reconstruction of the *M. sexta* V_1-ATPase (48, 50). Such protuberances are in an arrangement following

alternating subunits and might belong to the extended N termini of the three A subunits in the hexamer (7, 48).

In summary, the data presented demonstrate that subunit E of the vacuolar ATPase is a central stalk subunit that is catalytically active in a hybrid $\alpha_3\beta_3$EG-ATPase complex similar to subunit γ in F-ATPases. Such an arrangement, where E plays a role of a central stalk subunit, was recently proposed for the V_1-ATPase from mung bean (52). The reconstitution and structural analysis of a hybrid complex, like the presented $\alpha_3\beta_3$EG oligomer, proved to be essential for the elucidation of structural and functional homologies between subunits γ and E, which cannot be extracted from gene sequence alignments (3).

Acknowledgments—We thank A. Armbrüster (Universität des Saarlandes) for skillful technical assistance and Dr. T. R. M. Baerends for help with x-ray modeling. We thank Prof. M. Yoshida (Tokyo Institute of Technology, Yokohama) for the generous gift of the α and β subunits from TF_1 and Prof. H.-J. Schäfer (Universität Mainz) for support.

REFERENCES

1. Stevens, T. H., and Forgac, M. (1997) *Annu. Rev. Cell Dev. Biol.* **13,** 779–808
2. Nelson, N., and Harvey, W. R. (1999) *Physiol. Rev.* **79,** 361–385
3. Lolkema, J. S., Chaban, Y., and Boekema. E. J. (2003) *J. Bioenerg. Biomembr.* **35,** 323–335
4. Nishi, T., and Forgac, M. (2002) *Nat. Rev. Mol. Cell. Biol.* **3,** 94–103
5. Wieczorek, H., Brown, D., Grinstein, S., Ehrenfeld, J., and Harvey, W. R. (1999) *BioEssays* **21,** 637–648
6. Hilario, E., and Gogarten (1998) *J. Mol. Evol.* **46,** 703–715
7. Gogarten, J. P., and Taiz, L. (1992) *Photosynth. Res.* **33,** 137–146
8. Kasho, V., and Boyer, P. (1989) *Proc. Natl. Acad. Sci. U. S. A.* **86,** 8708–9711
9. Inoue, T., Wilkens, S., and Forgac, M. (2003) *J. Bioenerg. Biomembr.* **35,** 291–299
10. Grüber, G., Wieczorek, H., Harvey, W. R., and Müller, V. (2001) *J. Exp. Biol.* **204,** 2597–2605
11. Stock D., Gibbons C., Arechaga I., Leslie A. G., and Walker, J. E. (2000) *Curr. Opin. Struct. Biol.* **10.** 672–679
12. Pedersen, P. L., Hee Ko, Y., and Hong, S. (2000) *J. Bioenerg. Biomembr.* **32,** 325–332
13. Sun-Wada, G.-H., Wada, Y., and Futai, M. (2003) *J. Bioenerg. Biomembr.* **33,** 347–358
14. Müller, V., and Grüber, G. (2003) *Cell Mol. Life Sci.* **60,** 474–494
15. Wilkens, S., and Capaldi, R. A. (1998) *Biochim. Biophys. Acta* **1365,** 93–97
16. Rubinstein, J. L., Walker, J. E., and Henderson, R. (2003) *EMBO J.* **22,** 6182–6192
17. Boekema, E. J., van Breemen, J. F., Brisson, A., Ubbink-Kok, T., Konings, W. N., and Lolkema, J. S. (1999) *Nature* **401,** 37–38
18. Wilkens, S., Vasilyeva, E., and Forgac, M. (1999) *J. Biol. Chem.* **274,** 31804–31810
19. Domgall, I., Venzke, D., Luttge, U., Ratajczak, R., and Böttcher, B. (2002) *J. Biol. Chem.* **277,** 13115–13121
20. Dschida, W. J., and Bowman, B. J. (1992) *J. Biol. Chem.* **267,** 18783–18789
21. Svergun, D. I., Konrad, S., Huss, M., Koch, M. H. J., Wieczorek, H., Altendorf, K., Volkov, V. V., and Grüber, G. (1998) *Biochemistry* **37,** 17659–17663
22. Nelson, H., Mandiyan, S., and Nelson, N. (1995) *Proc. Natl. Acad. Sci. U. S. A.* **92,** 497–501
23. Bowman, E. J., Steinhardt, A., and Bowman, B. J. (1995) *Biochim. Biophys. Acta* **1237,** 95–98
24. Tomashek, J. J., Graham, L. A., Hutchins, M. U., Stevens, T. H., and Klionsky, D. J. (1997) *J. Biol. Chem.* **272,** 26787–26793
25. Chaban, Y., Ubbink-Kok, T., Keegstra, W., Lolkema, J. S., and Boekema, E. J. (2002) *EMBO Rep.* **3,** 982–987
26. Rizzo, V. F., Coskun, Ü., Radermacher, M., Ruiz, T., Armbrüster, A., and Grüber, G. (2003) *J. Biol. Chem.* **278,** 270–275
27. Grüber, G., Godovac-Zimmermann, J., Link, T. A., Coskun, Ü., Rizzo, V. F., Betz, C., and Bailer, S. M. (2002) *Biochem. Biophys. Res. Commun.* **298,** 383–391
28. Crider, B. P., Andersen, P., White, A. E., Zhou, Z., Li, X., Mattson, J. P., Lundberg, L., Keeling, D. J., Xie, X.-S., Stone, D. K., and Peng, S.-B. (1997) *J. Biol. Chem.* **272,** 10721–10728
29. Charsky, C. M., Schumann, N. J., and Kane, P. M. (2000) *J. Biol. Chem.* **275,** 37232–37239
30. Shirakihara, Y., Leslie, A. G., Abrahams, J. P., Walker, J. E., Ueda, T., Sekimoto, Y., Kambara, M., Saika, K., Kagawa, Y., and Yoshida, M. (1997) *Structure* **5,** 825–836
31. Ohta, S., Yohda, M., Hirata, H., Hamaotot, T., Otawara-Hamamoto, Y., Matsuda, K., and Kagawa, Y. (1988) *Biochim. Biophys. Acta* **933,** 141–155
32. Kagawa, Y., and Yoshida, M. (1979) *Methods Enzymol.* **55,** 781–787
33. Armbrüster, A., Bailer, S. M., Koch, M. H., Godovac-Zimmermann, J., and Grüber, G. (2003) *FEBS Lett.* **546,** 395–400
34. Laemmli, U. K. (1970) *Nature* **227,** 680–685
35. Schägger, H., Cramer, W. A., and v. Jagow, G. (1994) *Anal. Biochem.* **217,** 220–230
36. Arnold, A., Wolf, H. U., Ackermann, B., and Bader, H. (1976) *Anal. Biochem.* **71,** 209–213
37. Oostergetel, G. T., Keegstra, W., and Brisson, A. (1998) *Ultramicroscopy* **74,** 47–59
38. Frank, J., and Penczek, P. (1995) *Optik* **98,** 125–129
39. Dube, P., Bacher, G., Stark, H., Mueller, F., Zemlin, F., van Heel, M., and Brimacombe, R. (1998) *J. Mol. Biol.* **279,** 403–421
40. van Heel, M., and Frank, J. (1981) *Ultramicroscopy* **6,** 187–194
41. van Heel, M. (1984) *Ultramicroscopy* **13,** 165–184
42. Ludtke, S. J., Baldwin, P. R., and Chiu, W. (1999) *J. Struct. Biol.* **128,** 82–97
43. van Heel, M. (1987) *Ultramicroscopy* **21,** 95–100
44. Ishii, N., Yoshimura, H., Nagayama, K., Kagawa, Y., and Yoshida, M. (1993) *J. Biochem. (Tokyo)* **113,** 245–250
45. Jones, R. P., Hunt, I. E., Jaeger, J., Ward, A., O'Reilly, J., Barratt, E. A., Findlay, J. B., and Harrison, M. A. (2001) *Mol. Membr. Biol.* **18,** 283–290
46. Deleted in proof
47. Gibbons, C., Montgomery, M. G., Leslie, A. G., and Walker, J. E. (2000) *Nat. Struct. Biol.* **7,** 1055–1061
48. Radermacher, M., Ruiz, T., Wieczorek, H., and Grüber, G. (2001) *J. Struct. Biol.* **135,** 26–37
49. Kaibara, C., Matsui, T., Hisabori, T., and Yoshida, M. (1996) *J. Biol. Chem.* **271,** 2433–2438
50. Grüber, G., Radermacher, M., Ruiz, T., Godovac-Zimmermann, J., Canas, B., Kleine-Kohlbrecher, D., Huss, M., Harvey, W. R., and Wieczorek, H. (2000) *Biochemistry* **39,** 8609–8616
51. Arata, Y., Baleja, J. D., and Forgac, M. (2002) *J. Biol. Chem.* **277,** 3357–3363
52. Li, Z., and Zhang, X. (2004) *Planta*,in press